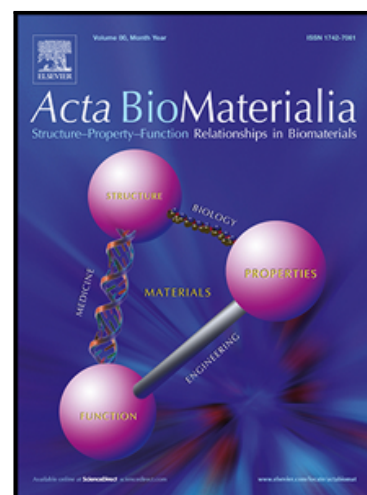


Adipose-derived stem cells with miR-150-5p inhibition laden in hydroxyapatite/tricalcium phosphate ceramic powders promote osteogenesis via regulating Notch3 and activating FAK/ERK and RhoA

Fanglin Wang , Qiao Wang , Yu Zhao , Zhiyu Tian , Shijie Chang , Hao Tong , Ningwei Liu , Shuling Bai , Xiang Li , Jun Fan

PII: S1742-7061(22)00643-2  
DOI: <https://doi.org/10.1016/j.actbio.2022.09.070>  
Reference: ACTBIO 8326



To appear in: *Acta Biomaterialia*

Received date: 5 April 2022  
Revised date: 24 September 2022  
Accepted date: 28 September 2022

Please cite this article as: Fanglin Wang , Qiao Wang , Yu Zhao , Zhiyu Tian , Shijie Chang , Hao Tong , Ningwei Liu , Shuling Bai , Xiang Li , Jun Fan , Adipose-derived stem cells with miR-150-5p inhibition laden in hydroxyapatite/tricalcium phosphate ceramic powders promote osteogenesis via regulating Notch3 and activating FAK/ERK and RhoA, *Acta Biomaterialia* (2022), doi: <https://doi.org/10.1016/j.actbio.2022.09.070>

This is a PDF file of an article that has undergone enhancements after acceptance, such as the addition of a cover page and metadata, and formatting for readability, but it is not yet the definitive version of record. This version will undergo additional copyediting, typesetting and review before it is published in its final form, but we are providing this version to give early visibility of the article. Please note that, during the production process, errors may be discovered which could affect the content, and all legal disclaimers that apply to the journal pertain.

© 2022 Published by Elsevier Ltd on behalf of Acta Materialia Inc.

**Adipose-derived stem cells with miR-150-5p inhibition laden in hydroxyapatite/tricalcium phosphate ceramic powders promote osteogenesis via regulating Notch3 and activating FAK/ERK and RhoA**

Fanglin Wang<sup>1#</sup>, Qiao Wang<sup>1#</sup>, Yu Zhao<sup>2#</sup>, Zhiyu Tian<sup>3</sup>, Shijie Chang<sup>4</sup>, Hao Tong<sup>1</sup>,  
Ningwei Liu<sup>5</sup>, Shuling Bai<sup>1</sup>, Xiang Li<sup>1,6\*</sup>, Jun Fan<sup>1\*</sup>

<sup>1</sup>Department of Tissue Engineering, School of Intelligent Medicine, China Medical University, No.77 Puhe Road, Shenyang North New Area, Shenyang, Liaoning Province, 110122, P.R. China

<sup>2</sup>Department of Plastic Surgery, Shengjing Hospital, Affiliated Hospital of China Medical University, No.36 Sanhao Street, Heping area, Shenyang, Liaoning Province, 110004, P.R. China

<sup>3</sup>Clinical Primary Department 105K, China Medical University, No.77 Puhe Road, Shenyang North New Area, Shenyang, Liaoning Province, 110122, P.R. China

<sup>4</sup>Division of Biomedical Engineering, China Medical University, No.77 Puhe Road, Shenyang North New Area, Shenyang, Liaoning Province, 110122, P.R. China

<sup>5</sup>5+3 integration of Clinical Medicine 106K, China Medical University, No.77 Puhe Road, Shenyang North New Area, Shenyang, Liaoning Province, 110122, P.R. China

<sup>6</sup>Department of Cell Biology, School of Life Sciences, China Medical University, No.77 Puhe Road, Shenyang North New Area, Shenyang, Liaoning Province, 110122, P.R. China

**Running title:** miR-150-5p inhibition enhances osteogenesis

# These three authors contribute equally to this work

**\*Address Correspondence to:**

Xiang Li MD, PhD

Email: cmu\_LX@163.com

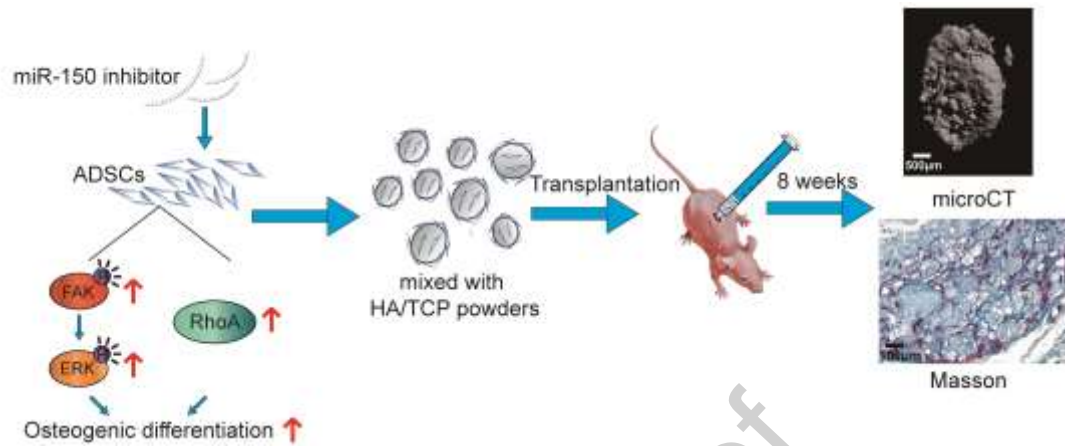
Jun Fan MD, PhD

E-mail: jfan@cmu.edu.cn

Department of Tissue Engineering, School of Intelligent Medicine,  
China Medical University, No.77 Puhe Road, Shenyang North New Area, Shenyang,  
Liaoning Province, 110122, P.R. China

**Disclosures:** Nothing to disclose

## Graphical Abstract



### Statement of Significance

Osteoporosis is a common chronic metabolic bone disease in humans. Bone tissue engineering based on mesenchymal stem cells, biomaterials, and growth factors, provides a promising way to treat osteoporosis and bone defects. ADSCs commonly differentiate into adipose cells, they can also differentiate into osteogenic cell lineages. Nucleic acids and protein have usually been considered as regulators of ADSCs osteogenic differentiation. In the current study, we demonstrated the combination of ADSCs with miR-150-5p inhibition and hydroxyapatite/tricalcium phosphate ceramic powders enhanced bone regeneration. Furthermore, miR-150-5p/Notch3 axis regulating osteogenesis via the FAK/ERK1/2 and RhoA pathway was assessed. The current study showed the application of ADSCs in bone regeneration might be a promising strategy for osteoporosis and bone damage repairing.

## Abstract

Adipose-derived mesenchymal stem cells (ADSCs) are multipotent stromal cells and play huge role in forming and repairing bone tissues. Emerging evidence shows that MicroRNAs (miRNAs) are involved in ADSCs differentiation. Here, we explored the role of *miR-150-5p* and its related mechanisms in ADSCs osteogenesis. Real-time PCR was used to determine *miR-150-5p* expression during ADSCs osteogenesis. *miR-150-5p* inhibitors, *miR-150-5p* ADV or short hairpin RNA (shRNA) of Notch3 were transfected to ADSCs for analyzing the effects on osteogenesis. The mixture of hydroxyapatite/tricalcium phosphate (HA/TCP) ceramic powders and transfected ADSCs was implanted into BALB/C nude mice. Micro-CT and histological methods were performed to evaluate the new bone formation. Compared with negative control (NC) and *miR-150-5p* overexpression, inhibition of *miR-150-5p* increased ADSCs osteogenesis by regulating Notch3. *MiR-150-5p* overexpression decreased the expression of pFAK, pERK1/2, and RhoA, while these were up-regulated when *miR-150-5p* was inhibited, or notch3 was silenced. Furthermore, *miR-150-5p* inhibition partially reversed the suppression effect of notch3 knockdown on osteogenesis *in vitro* and *in vivo*. This study demonstrated the critical function of *miR-150* during osteogenesis. The combination of ADSCs with *miR-150-5p* inhibition and HA/TCP might be a promising strategy for bone damage repair.

**Keywords:** ADSCs, miR-150, differentiation, osteogenesis, biomaterials

## 1.Introduction

Bone defects like fractures and fragility of bones, caused by osteoporosis, are the common injuries seen in hip, wrist, proximal humerus, or vertebrae in humans [1]. Osteoporosis is a kind of chronic metabolic bone disease. Bone tissue engineering (BTE) based on mesenchymal stem cells (MSCs), engineering materials, and growth factors (GFs), provides a promising alternative to treat osteoporosis and critical-sized bone defects [2]. Adipose-derived mesenchymal stem cells (ADSCs) are multipotent stromal cells, which can differentiate into multiple lineages, such as osteoblasts, chondrocytes, and adipocytes [3]. For their plasticity and low immunogenic potential, ADSCs have been extensively used in cell-based therapy for tissue repair and regeneration [4-6]. As known, ADSCs commonly differentiate into adipose cells, they can also differentiate into bone cells [5, 7, 8]. This differentiation mechanism has not been completely elucidated.

MiRNAs are a class of endogenous single-stranded non-coding RNAs (ncRNAs), which were discovered in nematodes and acted as key regulators of biological processes [9]. They can play synergistic and antagonistic actions in regulating cell differentiation, development, and homeostasis [10-12]. MiRNAs are also an emerging class of therapeutic drugs in some diseases [13, 14]. Recent studies showed that miRNAs level was changed in bone regeneration [15-18], indicating the potential effects of miRNAs in osteogenesis. *MiR-150-5p* was first detected to be related to chronic lymphocytic leukemia [19], and showed significantly differential expression in the visceral adipose tissue [20]. A recent study has suggested that *miR-150-5p* can modulate the osteoblast matrix mineralization in the mouse osteoblast cell line MC3T3-E1 [21]. Likewise, the up-regulated *miR-150-5p* level encouraged by tumor necrosis factor-alpha (TNF- $\alpha$ ) represses osteogenesis in bone marrow-derived mesenchymal stem cells (BMSCs) through modulating  $\beta$ -catenin [22]. Our recent study showed that *miR-150-5p* inhibition could enhance ADSCs proliferation [23].

The Notch family contains four transmembrane Notch receptors (Notch1-Notch4) and five canonical ligands (Jagged1, Jagged2, Delta-like1, Delta-like3, and Delta-like4),

which plays fundamental roles in balancing proliferation versus differentiation [24, 25]. In cell differentiation, Notch3 is the primary decider of cell lineage fate [26]. Our previous experiment has demonstrated that *miR-150-5p* promotes adipogenesis in ADSCs by targeting Notch3 [23].

The study indicates that Notch3 may be associated with the activation of ERK1/2 [27-29]. ERK is a regulator of early osteoblast and osteoclast differentiation, which is related to osteoclast survival, motility, and cell polarity [30]. In further, ERK is a crucial target of FAK [31]. Activation of FAK/ERK signaling pathways promoted osteogenic differentiation in ADSCs [32]. Several cell surface receptors can activate FAK and then subsequently play an essential character in the process of cell survival, proliferation, migration, and invasion [33]. The Rho/Rho-associated protein kinase (Rho/ROCK) pathway mediating differentiation is correlated with the morphological change of MSCs [34]. RhoA has been proved to influence MSC lineage allocation and regulate adipogenesis [35]. However, whether *miR-150-5p*/Notch3 axis can regulate FAK and RhoA is not known.

In this study, we investigated the effect of transplantation of miR-150 modified ADSCs laden in (HA/TCP) ceramic powders on osteogenesis, and explored the potential mechanisms. Specifically, *miR-150-5p*/Notch3 axis regulating osteogenesis via the FAK/ERK1/2 and RhoA pathway was assessed. Clarifying the fundamental mechanisms that direct the osteogenesis of ADSCs will give deeper insights into the regulatory patterns.

## 2. Materials and methods

### 2.1 ADSCs culture

ADSCs were kindly provided by Stem Cell Bank, the Chinese Academy of Sciences. Under sterile conditions, the ADSCs were cultured in DMEM/F-12 (Gibco, USA) with certified fetal bovine serum (10%, v/v, FBS qualified for Mesenchymal Stem Cells, Biological Industries, ISR) and penicillin-streptomycin solution (1%, v/v, Procell, China)

in a humidified incubator (Thermo, USA) at 37 °C with 5% CO<sub>2</sub>. The ADSCs were passaged after 80% confluence, and the culture medium was changed every 3 days. The five-passage cells were used in the further experiments. The phenotype of ADSCs were assessed by using a serial of markers.

## **2.2 Characterization of ADSCs by flow cytometry**

The ADSCs phenotype was identified by native markers (CD34 and CD45) and positive markers (CD44 and CD105) using flow cytometry as our previous study [23]. The five-passage ADSCs were stained for CD34, CD45, CD44, or CD105 (BD Pharmingen, USA) with fluorophore-conjugated antibodies at 4°C for 30 min. After washing with PBS, the cells were assed using fluorescence-activated cell sorting (FACS) analysis. Gating strategy was determined based on isotype control staining.

## **2.3 Osteogenic differentiation of ADSCs**

When ADSCs reached the density of 70–80%, the original medium was changed into the osteogenic induced medium with 50mg/L additional ascorbic acid (Sigma-Aldrich, USA), 0.1µmol/L dexamethasone (Solarbio, China), and 10mmol/L β-glycerophosphate (Sigma-Aldrich, USA). Termination of cell cultures occurred on day 0, 3, 7, 11, 14 for RNA isolation. Protein extraction, alkaline phosphatase (ALP) activity, and ALP staining were performed on day 7. Alizarin Red S staining was performed to detect positive calcium deposition on day 21.

## **2.4 Small Molecule Inhibitors.**

The ADSCs were starved for 24 h in DMEM/F-12 without FBS before treatment. FAK signaling were inhibited using PF-562271 (100nM , beyotime, China). Inhibition of ERK1/2 activation was conducted with ISRIB (100nM , beyotime, China) , and RhoA signaling were inhibited using CCG-1423 (10µM , Shanghai yuanye, China). The ADSCs without the inhibitors were used as controls.

## **2.5 RNA preparation and quantitative real-time polymerase chain reaction (RT-PCR) analysis**

Total RNAs were isolated from ADSCs using TRIzol Reagent (Takara, Japan). RNA quantities and qualities were measured using a BioDrop spectrophotometer (Biodrop, UK). To calculate the expression level of *miR-150-5p*, a specific primer of *miR-150-5p* for the stem-loop reverse transcription and a riboSCRIPT Reverse Transcription Kit (RiboBio, China) were used. Quantitative real-time PCR analysis was performed using primers, synthesized cDNAs, double-distilled water (ddH<sub>2</sub>O), and TB Green<sup>TM</sup> Premix Ex Taq<sup>TM</sup> II (Takara, Japan). A Light Cycler 480 (Roche, USA) performed the real-time quantitative PCR amplification with triplicate 20- $\mu$ L volume per reaction. For normalizing the relative expression of *miR-150-5p*, U6 was used as the internal control. The levels of *miR-150-5p* and U6 were assessed by the  $2^{-\Delta\Delta CT}$  method. Specific *miR-150-5p* primers for the stem-loop reverse transcription quantitative and RT-PCR amplification were purchased from RiboBio, China.

## 2.6 Cell transfection

*Hsa\_miR\_150-5p inhibitor and its respective negative control (NC) were provided by Pharma, China.* Transfection was performed in the presence of transfection reagent Lipofectamine<sup>TM</sup> 3000 reagent (Invitrogen, USA). The ADSCs were transfected with inhibitors or NC at a density of 70–80% in 6-well plates. The sequence of *hsa\_miR\_150-5p inhibitor* was: 5'-CACUGGUACAAGGGUUGGGAGA-3'. The sequence of *hsa\_miR\_150-5p NC* was: 5'-CAGUACUUUUGUGUAGUACAA-3'. The cells were applied for additional experiments after transfection for 48 h.

*Hsa\_miR\_150-5p overexpression adenovirus (ADV) and its NC were provided by Vigenebio, China.* The sequence of *hsa\_miR\_150-5p ADV* was: 5'-UCUCCCAACCCUUGUACCAGUG-3'. After being transfected for 48 h, the GFP fluorescence intensity was observed by fluorescent inverted microscope (Olympus, Japan) and the cells were obtained for additional experiments. Lentiviruses contain shRNA were used to knock down *Notch3*, the sequences of *shR-Notch3* were: shR-GFP, 5'-GCACCCAGTCCGCCCTGAGCAAATTCAAGAGATTTGCTCAGGGCGGACTGG

GTGCTTTTT-3'; *shR-Notch3-1*,  
 5'-GATCCGCGTGTGTAGACGGTGTCAATATTCAAGAGATATTGACACCGTCTACA  
 CACGTTTTTTA-3'; *shR-Notch3-2*,  
 5'-GATCCGCTAGCTTCTCGTGCTTGTTC AAGAGAACAAGCACACGAGAAGCTA  
 GCTTTTTTA-3'; *shR-Notch3-3*,  
 5'-GATCCGGACAAGATGCACTGGGAATGTTCAAGAGACATTCCCAGTGCATCTT  
 GTCCTTTTTTA-3'. The transfected ADSCs were obtained for additional experiments  
 after transfection for 48 h. After transfection for 48 h, GFP fluorescence intensity was  
 observed by fluorescent inverted microscope (Olympus, Japan). To build  
 lentiviral-mediated stable knockdown of *Notch3*, we used 1.5µg/mL Puromycin  
 Dihydrochloride (beyotime, China) to filter transfected cells. *ShR-Notch3* stable  
 knockdown ADSCs were applied for additional experiments.

## 2.7 Western blot analysis

After transfection or osteogenic induction, ADSCs were used to crack protein for western blot analysis. Total cell lysates were prepared by RIPA lysis buffer (RIPA, comprising NP40 and sodium deoxycholate, Beyotime, China) at 4°C for 10 min to extract total proteins, with 1% phenylmethanesulfonyl fluoride (PMSF, Beyotime, China) and 1% phosphatase inhibitor (Beyotime, China). Total cell lysates are collected in a 1.5mL tube, crushed by 5s ultrasound at 10s interval and centrifuge at 4°C, 12000rpm 30min. Equal amounts of proteins were separated with sodium dodecyl sulphate–polyacrylamide gel electrophoresis (SDS-PAGE). 0.45µm poly-vinylidene fluoride (PVDF) membranes (GE Amersham, USA) were used to transfer proteins from gel. The membranes were blocked by non-fat milk (5%, w/v) for 2 h at room temperature. The appropriate primary antibodies were used to incubate the blots at 4°C overnight. After being washed by PBS three times, the blots were incubated with HRP polymer secondary antibodies for 1 h. Chemiluminescence was sensed with Tanon™ High-sig ECL Western Blotting Substrate (Tanon, China). Images were acquired with an automatic chemiluminescence image analysis system

(Tanon, China) and evaluated by Image J software (National Institutes of Health, USA). Primary antibodies in this study were used against RUNX-2 (Bioss, China), Osteocalcin (Abclonal, China), collagen type I alpha 1 (COL1A1, Bioss, China), Notch3 (Santa Cruz, USA), pFAK (Bioss, China), FAK (Cell Signaling Technology, USA), pERK1/2 (Bioss, China), ERK1/2 (Bioss, China), RhoA (Proteintech, USA), and glyceraldehyde-3-phosphate dehydrogenase (GAPDH, Proteintech, USA) as loading control.

## 2.8 Bone formation *in vivo*

In this study, all animal procedures were approved by the Laboratory Animal Welfare and Ethical Review of China Medical University (IACUC Issue No. CMU2020106). Eight-week-old female BALB/C nude (nu/nu) mice (n=32) were procured from HFK Biotechnology (Beijing, China). The ADSCs transfected with miR-150 overexpression ADV, miR-150 inhibitor and/or shR-Notch3, or non-transfected ADSCs (NC) were prepared. National Engineering Research Center for Biomaterials, China, provided hydroxyapatite/tricalcium phosphate (HA/TCP) ceramic powder for this experiment. The HA/TCP ceramic powders are consisted of 60% hydroxyapatite and 40% tricalcium phosphate. The grain size of HA/TCP powders is 50-80 $\mu$ m. Before cell seeding, the HA/TCP ceramic powders (40 mg) were wetted with 1 ml control growth medium and incubated overnight. Then, the cultured ADSCs were trypsinized. A total of  $2 \times 10^6$  ADSCs (in 200  $\mu$ L medium) were mixed with wetted HA/TCP granules (40mg) and incubated at 37°C overnight in 5% CO<sub>2</sub>. The HA/TCP granules without any cells were used as a control. The mixture was implanted into the dorsal surface of BALB/C-nu/nu mice. Two mid-longitudinal skin incisions of about 1 cm in length on the dorsal surface of each mouse were made, and subcutaneous pouches by blunt dissection were created on each mouse. Two implants were placed in each mouse. Then, the incisions were closed with surgical sewing. Eight parallel implants of each group were placed randomly on 8 mice. The implants were distributed randomly over the mice and over the two different implant positions. They were randomly divided into

eight groups, i.e., HA/TCP group (HA/TCP without ADSCs), miR-150 overexpression negative control (NC) group, miR-150 inhibitor NC group, shR NC group, miR-150 overexpression group, miR-150 inhibitor group, shR-Notch3 group, shR-Notch3+miR-150 inhibitor group. The mice were housed in SPF facility with controlled room temperature and humidity under a 12 h light/12 h dark cycle. The implants were harvested at 8 weeks postoperatively.

### **2.9 Micro-computed tomography (micro-CT) analysis**

New bone formation in implants were scanned using Skyscan1276 Micro-CT (Bruker, Germany) at 55 kV, 200  $\mu$ A, 386 ms, and an adequate pixel size of 17.520  $\mu$ m. All scanned images were reconstructed into 3-dimensional images using CTvox software (Bruker, Germany). The ratio of bone volume/tissue volume (BV/TV) was determined.

### **2.10 Hematoxylin and eosin (H&E) staining**

The implants were harvested at 8 weeks and then fixed in paraformaldehyde (4%, v/v). Then the samples were decalcified in EDTA (10%, w/v, pH 8.0) for 14 days. The implants were decalcified and embedded in paraffin. Sections were cut at 7  $\mu$ m and performed with H&E and Masson's trichrome staining. The images were attained by an upright microscope (Olympus, Japan).

### **2.11 Immunohistochemistry staining**

The antigen of specimens was retrieved by a high pH Tris-EDTA buffer. After being blocked with bovine serum albumin (3%, w/v BSA, Boster, China) for 30 min at 37 °C, the sections were incubated with primary RUNX-2 antibody (Bioss, China) and collagen type I alpha 1 (COL1A1, Bioss, China) overnight at 4 °C. The slices were incubated with the HRP polymer secondary antibody for 1h at 37 °C. 3,3'-diaminobenzidine (DAB) was used for traditional detection, which precipitates a brown color on the tissue. Hematoxylin was used as a counterstain to stain nuclei. Images were captured with the upright microscope (Olympus, Japan).

### 2.12 ALP activity

ALP quantitative analysis was used to accurately determine the mineralization of ADSCs. The proteins of differentiated cells in 6-well plates were isolated and determined their concentration by BCA Protein Assay Kit (Beyotime, China). Configured the reagent and incubated it at 37°C for 10 minutes based on the manufacturer's protocol of Alkaline Phosphatase Assay Kit (Beyotime, China). A microplate reader (Thermo, USA) was used to measure the absorbance at a wavelength of 405 nm. Calculated the ALP activity according to concentration and absorbance.

### 2.13 ALP staining and Alizarin red staining

The osteogenic induced cells in 12-well plates were fixed by paraformaldehyde (4%, v/v) for 15 min. Followed by three times washes with distilled water, osteogenic induced ADSCs were stained with ALP staining kit (Beyotime, China) for 3 h in a 37°C incubator. Captured the pictures under an inverted microscope (Olympus, Japan), ALP-positive cells were stained in purple color. Similarly, the fixed ADSCs were stained with 1% Alizarin Red-S staining solution (Solarbio, China) for 30 min to detect the formation of mineralized nodule.

### 2.14 Immunofluorescence

A total of  $3 \times 10^4$  ADSCs were loaded on each cell climbing in a 6-wells plate and transfected with *hsa\_miR\_150-5p* inhibitor and ADV. After washes with phosphate buffered saline (PBS) three times (5 min each time), transfected ADSCs were fixed with paraformaldehyde (4%, v/v) for 15 minutes. They were permeabilized with Triton X-100 (0.1%, v/v) for 5 minutes, and blocked with 5% goat serum for 1 h at RT. The cells were incubated with primary antibodies(dilution of 1:200) overnight at 4°C, followed by fluorescent secondary antibody(dilution of 1:1000) for 1 h at 37°C. Followed by three times washes with PBS, DAPI counterstained the cells for 5 min at

room temperature (RT). Images of stained cells were captured with a fluorescence confocal microscope (Olympus, Japan). Primary antibodies in this study were used against RUNX-2 (Bioss, China), pFAK (Bioss, China), pERK1/2 (Bioss, China), RhoA (Proteintech, USA), and F-actin (Abcam, USA).

### 2.15 Statistical analysis

All experiments were conducted at least three times. Data were analyzed using the Prism 8 software (GraphPad Software, USA). The results were expressed as *mean*  $\pm$  *SEM*. One-Way Analysis of Variance (ANOVA) and *student's unpaired t-test* were used to evaluate the significance of any differences. A value of  $*p < 0.05$ ,  $**p < 0.01$ , and  $***p < 0.001$  obtained from *t-test* was accounted statistically significant.

## 3. Results

### 3.1 *MiR-150-5p* was associated with the osteogenic differentiation of ADSCs

Firstly, the phenotype of ADSCs was identified. Flow cytometry showed that ADSCs were positive for surface markers CD44 and CD105, and negative for CD34 and CD45 (Fig 1S). ADSCs with certain conditions can differentiate into multiple cell types. To identify *miR-150-5p* expression with relevant functions in osteogenesis, we performed real-time PCR analysis on ADSCs after osteogenic induction at 1,3,7,11, and 14 days. The *miR-150-5p* expression decreased from the first day until the 14th day after osteogenic induction and reached the platform period on the 7th day (Fig. 1). This result suggested that *miR-150-5p* is downregulated during osteogenic induction and is involved in the ADSCs osteogenesis.

### 3.2 *MiR-150-5p* inhibited the osteogenic differentiation of ADSCs

To characterize the mechanism of *miR-150-5p* on regulating osteogenesis, the gain-of-function and loss-of-function studies were conducted in ADSCs. First, the ADSCs were infected with adenovirus (ADV)-*miR-150-5p* or its negative control (NC). After 7 days of osteogenic induction with osteogenic induced medium (OM), we measured osteogenic markers COL1A1, Runt-related transcription factor 2 (RUNX-2),

and Osteocalcin, as the criterion for evaluating the osteogenic effect. It showed that overexpression of *miR-150-5p* significantly inhibited the expression of COL1A1, RUNX-2 and Osteocalcin (Fig. 2A). Alkaline phosphatase (ALP) activity and ALP staining also demonstrated that *miR-150* overexpression could decrease osteogenic differentiation in ADSCs (Fig. 2B). Consistently, Alizarin Red-S staining showed that the area of mineralized nodule formation was decreased in ADSCs with *miR-150-5p* overexpression compared with control ADSCs (Fig. S2A). Meanwhile, miRNA inhibitor was used to inhibit *miR-150-5p* function by explicitly binding mature miRNAs in the cytoplasm. After osteogenic differentiation for 7 days, Western blot result showed that the level of COL1A1, RUNX-2 and Osteocalcin was obviously increased when the *miR-150* function was inhibited (Fig. 2C). Furthermore, ALP activity was also significantly increased with inhibition of *miR-150-5p* (Fig. 2D). The area of mineralized nodule formation was also increased in ADSCs with inhibition of *miR-150-5p* compared with control ADSCs (Fig. S2B). The above results concluded that *miR-150-5p* was a negative regulator in ADSCs' osteogenic differentiation.

### **3.3 *MiR-150-5p* inhibition promoted osteogenesis *in mice***

To confirm the inhibitory effects of *miR-150-5p* on the osteogenic differentiation of ADSCs *in vivo*, BALB/C-nu/nu mice were used to simulate the clinical application of tissue-engineered bone implanted with ADSCs in humans. Different transfected ADSCs mentioned above were cultured with hydroxyapatite/tricalcium phosphate (HA/TCP) ceramic powders respectively. Immunofluorescence microscopy showed that GFP labeled ADSCs grew around the HA/TCP powder (Fig. 3A). Then, the mixture of ADSCs and HA/TCP ceramic powders was implanted into the dorsal surface of BALB/C nude mice (Fig. 3B). Eight weeks after transplantation, the implants were evaluated *in vivo* by microcomputed tomography (micro-CT) (Fig. 3C). The new bone formed in the *miR-150-5p* inhibitor group exhibited a faster regeneration rate than the NC group. The regeneration of new bone in *miR-150-5p* overexpression and the shR-Notch3 group was much less compared with the NC group (Fig. 3D).

Then, the implants were harvested and treated with decalcification for histological staining. Hematoxylin-eosin (H&E) staining exhibited the overall structure of the implants (Fig. 4A). HA-TCP of the implants was extensively absorbed in the *miR-150-5p* inhibitor group, and many red-stained osteoid-like tissues were observed. Masson trichrome staining of implants revealed a more collagen-positive area (blue) in the *miR-150-5p* inhibition group (Fig. 4A, B). Additionally, immunohistochemistry results showed that COL1A1 and RUNX-2 (brown) expression was increased with *miR-150-5p* inhibition and was decreased by *miR-150-5p* overexpression (Fig. 4A, 4C). However, the level of COL1A1 and RUNX-2 in the shR-Notch3+*miR-150-5p* inhibition group were higher than the shR-Notch3 group, but lower than that in the *miR-150-5p* inhibition group. Taken together, the *miR-150-5p* inhibition in ADSCs improved osteogenesis. It is concluded that inhibition of *miR-150-5p* could promote osteogenic differentiation of ADSCs by regulating Notch3 *in vivo*.

#### **3.4 *MiR-150-5p* regulated the expression of Notch3, FAK/ERK, and RhoA in ADSCs**

The potential signaling pathway was evaluated to elucidate the mechanism underlying *miR-150-5p* role in mediating the impairment of ADSCs osteogenesis. Notch3, as the target of *miR-150*, is downregulated with *miR-150* overexpression and up-regulated with *miR-150* inhibition. FAK is a non-receptor protein tyrosine kinase that plays a decisive role in cellular focal adhesions and cell contacts within the extracellular matrix [36]. RhoA, a well-characterized regulator of cytoskeletal organization [37]. Relying on the transfected cells established above, the expression of FAK, ERK1/2, and their phosphorylated form were detected by immunofluorescence and Western blot (Fig. S3A, B and Fig. 5). pFAK was in the nucleus, while pERK1/2 was expressed in the nucleus and cytoplasm. *MiR-150-5p* overexpression could downregulate the protein level of pFAK and pERK1/2. In contrast, pFAK and pERK1/2 were up-regulated and transferred to the cytoplasm by inhibiting the level of *miR-150-5p*. While the basal level of total FAK and ERK1/2 was unchanged. It suggested that

*miR-150-5p* could modulate cell adhesion by regulating the phosphorylation of FAK and ERK1/2. Simultaneously, Western blot analysis showed that *miR-150-5p* overexpression decreased expression RhoA and *miR-150-5p* inhibition affected oppositely (Fig. 5). It revealed that *miR-150-5p* might regulate cell adhesion and initiation of early osteogenic differentiation.

### **3.5 Notch3 knockdown could downregulate the phosphorylation of FAK and ERK1/2 and inhibit the osteogenic differentiation of ADSCs**

In our previous study, results of dual-luciferase reporter assay revealed that *miR-150-5p* had a binding sequence with the mutated seed match site in the 3'UTR region of Notch3 and repressed its expression [23]. However, whether Notch3 could regulate osteogenesis of ADSCs was still unknown. To study the potential role of Notch3 in ADSCs during osteogenic differentiation, three lentiviruses containing short hairpin RNA (shRNA) were transfected into ADSCs to knockdown Notch3 (Fig. 6A). The results showed that the Notch3 knockdown efficiency of *shR-Notch3-2* and *shR-Notch3-3* were better than *shR-Notch3-1*. Then the *shR-Notch3-2* were chosen for further exploring the role of Notch3 on osteogenic differentiation. Western blot and immunofluorescence showed that knockdown of Notch3 decreased expression of pFAK and pERK1/2 without affecting the expression of total FAK and ERK. The expression of RhoA was also decreased with Notch3 knockdown (Fig. 6B and Fig. S3C). With osteogenic differentiation for 7 days, the expression of COL1A1, RUNX-2 and Osteocalcin was significantly downregulated by knockdown of Notch3 compared with that in the negative control group (Fig. 6C). ALP activity and staining analysis also revealed that knockdown of Notch3 could decrease osteogenic differentiation in ADSCs (Fig. 6D). Alizarin Red-S staining further showed that the area of mineralized nodule formation was decreased in ADSCs with Notch3 knockdown (Fig. S4). The above results suggested that Notch3 knockdown could inhibit osteogenic differentiation and repress phosphorylation of FAK and ERK1/2, and the expression of RhoA.

### 3.6 Inhibition of *miR-150-5p* could enhance FAK and RhoA signaling pathway through regulating Notch3 expression in osteogenesis of ADSCs

To further clarify whether *miR-150-5p*/Notch3 was involved in regulating pFAK/pERK1/2 and RhoA, the *miR-150-5p* inhibitor was transfected to ADSCs with Notch3 knockdown. After osteogenic differentiation for 7 days, the expression level of COL1A1, RUNX-2 and Osteocalcin was downregulated with Notch3 knockdown as above and regulated back to approximative but insufficient normal levels after *miR-150-5p* were inhibited (Fig. 7A). ALP activity and staining also revealed that osteogenic differentiation of ADSCs was repressed by knockdown of Notch3 and regulated back after *miR-150-5p* inhibition (Fig. 7B). Interestingly, the area of mineralized nodule was reduced significantly in ADSCs with Notch3 knockdown, which was largely rescued by *miR-150-5p* inhibition (Fig. S5). It revealed that the inhibition of *miR-150-5p* up-regulated the osteogenic differentiation inhibited by Notch3 knockdown. To further realize its potential mechanism, the expression of FAK and RhoA was detected through Western blot analysis. The level of pFAK and pERK1/2, which was down-regulated after Notch3 knockdown, was up-regulated with *miR-150-5p* inhibition (Fig. 7C). This indicated that Notch3 mediated *miR-150-5p* regulating pFAK and pERK1/2 signal, and participated in the early osteogenic differentiation. RhoA was also downregulated due to the knockdown of Notch3 and then up-regulated due to the inhibition of *miR-150-5p* (Fig. 7C). It showed that *miR-150-5p* regulated the expression of RhoA and modulated cytoskeletal organization via Notch3. To determine the cascade of FAK/ERK and RhoA, ADSCs were treated with each inhibitor for ERK, FAK and RhoA. As shown in Fig. S6, FAK inhibitor (PF562271) treatment significantly inhibited the expression of pFAK and pERK1/2, and RhoA expression was not changed. However, ERK inhibitor (ISRIB) and RhoA inhibitor (CCG-1423) just inhibited the expression of pERK1/2 and RhoA in ADSCs respectively. This result showed that FAK could regulate ERK expression. Taken together, these results revealed that inhibition of *miR-150-5p* could activate the

pFAK/pERK1/2 and RhoA signaling pathway by regulating Notch3 expression and promote the osteogenic differentiation of ADSCs.

#### 4. Discussion

Osteogenic differentiation is one of the critical parts of cell lineage commitment of ADSCs, and it is the theoretical basis for the clinical application of tissue engineering bone and bone injury repair. MiRNA is an epigenetic regulator in developmental timing, cell death, proliferation, and differentiation. However, the mechanism of miRNA regulating osteogenesis of ADSCs is largely unknown. Our study provided new evidence that *miR-150-5p* modulated osteogenic differentiation of ADSCs by regulating Notch3 expression. Notch3 could regulate the phosphorylation of the FAK/ERK1/2 signaling pathway. In addition, *miR-150-5p* could regulate RhoA through Notch3, thereby regulating cytoskeletal construction and osteogenesis in ADSCs.

MiRNAs are a group of endogenous non-coding RNA, which can induce specifically targeted mRNA degradation or repression [38]. Some miRNAs have been shown to play a significant role in osteogenic differentiation process [15-18]. As reported, *miR-150* was suggested to be correlated with osteogenesis process [39]. *MiR-150* negatively affects osteoblasts and positively affects osteoclasts by modulating osteoactivin/GPNMB expression [40]. In the current study, inhibition of *miR-150-5p* considerably increased the expression of Notch3 and improved ADSCs osteogenesis. In contrast, overexpression of *miR-150-5p* or Notch3 silence repressed the commitment of osteocytes. Notch3 is a Notch family member, as receptors play a significant role in both T-cell differentiation and leukemogenesis [41, 42]. Our previous study found that *miR-150-5p* post transcriptionally regulated Notch3 mRNA with a 7 nt match site complementary in the 3'UTR sequence [23]. Based on the above results, we speculate that *miR-150-5p* / Notch3 axis is also involved in the osteogenesis of ADSCs. In further, transfection of miR-150 also reduced the osteogenic differentiation in bone marrow mesenchymal stem cells [22]. On the other hand, one in vitro study showed that miR-150 could promote bone matrix mineralization in mouse osteoblastic

cell line MC3T3-E1[21]. However, miR-150 knockout mice demonstrated increased osteoblast differentiation and decreased osteoclastogenesis [43]. Taken together, these are likely the different roles of miR-150 in modulating bone formation processes due to the cell's types or the stages of osteoblast development. The more detailed mechanism on miR-150 regulating osteogenic differentiation of ADSCs needs to be further investigated in later study.

Not only clarifying the fundamental mechanisms that direct the osteogenesis of ADSCs, the experiment was also performed *in vivo*. HA/TCP is biphasic calcium phosphates bioceramics (BCP), recently accepted as bone defect filler by the European Community (EC label). It substitutes as a valuable graft in the field of tissue engineering [44]. HA/TCP performs osteoinductive potential and can trigger ADSCs toward osteogenic differentiation [45]. In current study, ADSCs with miR-150-5p inhibition were loaded on HA/TCP for implantation in BALB/C-nu/nu mice. HA/TCP scaffold supplied mechanical stability and actively supported ADSCs differentiating into osteoblasts and new bone formation. ADSCs with *miR-150-5p* inhibition obviously promoted bone mineralization, and the expression of osteogenic factors (COL1A1 and RUNX-2) in mice.

Furthermore, *miR-150-5p*/Notch3 axis regulating FAK/ERK1/2 and RhoA pathway was determined. Notch3 is associated with activation of extracellular-signaling-regulated kinase 1/2 (ERK1/2) and mitogen-activated protein kinase (MAPK) phosphatase 1 (MKP-1) [28, 29]. Activation of FAK is early events following integrin–extracellular matrix engagement [46]. ERK phosphorylation is crucially dependent on FAK activation [31]. FAK and ERK1/2 play an essential role in cell adhesion in early osteogenic differentiation. A previous study has demonstrated that the activation of the FAK/ERK pathway promoted osteogenic differentiation in ADSCs [32]. In addition, cell surface receptors can activate FAK signal [33]. Interestingly, we verified that knockdown of Notch3 could decrease the phosphorylation of FAK and ERK1/2 while no change in their basal expression. As the process of osteogenic differentiation, cytoskeleton construction is the most critical

step in forming osteocyte morphology. RhoA/ROCK pathway mediates differentiation with the ability for lineage switch in MSCs [47]. RhoA was mainly located in the cytoplasm. Its expression was increased by inhibiting *miR-150-5p*, which indicated the construction of the cytoskeleton. *MiR-150-5p* regulated cytoskeletal organization by acting on nuclear-cytoplasmic redistribution of RhoA. FAK and RhoA are two cooperative pathways, that respectively regulate osteogenic differentiation in cytoskeleton formation and cell adhesion. By these signaling pathways, F-actin was increased, which was essential for actin cytoskeleton structural integrity and drove osteogenic differentiation. Inhibition of *miR-150-5p* directly led to the increase of Notch3 and promoted FAK/ERK and RhoA signaling pathways. With the upregulation of ALP and RUNX-2 in ADSCs with *miR-150-5p* inhibition, the ADSCs differentiated into osteogenic fate.

## 5. Conclusions

This work reveals a previously unidentified effect of *miR-150-5p* inhibition in promoting osteogenic differentiation in ADSCs. The promoting effect may be mediated by regulating FAK/ERK1/2 and RhoA pathway via Notch3. *In vivo* experiments presented that ADSCs with *miR-150-5p* inhibition enhanced bone regeneration. Therefore, the combination of ADSCs with *miR-150-5p* inhibition and HA/TCP might be a promising strategy for osteoporosis and bone damage repair.

## Author contributions

FLW performed the experiments, data analysis and wrote the manuscript. QW participated in performing the experiments and data analysis. FLW and YZ performed animal surgery and care. ZYT, SJC, HT, and NWL provided technical support. XL conceived and participated in revising the manuscript. SLB supervised the study. JF conceived and designed the study, and participated in writing the manuscript.

## Declaration of conflicting interests

The authors declare that we have no conflict of interest.

## **Acknowledgments**

This work was supported by Liaoning Revitalization Talents Program, China [no. XLYC1907124] and the National Natural Science Foundation, China [no. 81571919].

## **Ethical approval**

All animal procedures were conducted in accordance with the protocol approved by the Laboratory Animal Welfare and Ethical Review of China Medical University (IACUC Issue No. CMU2020106).

## **Data availability**

All data supporting this study's findings are available from the corresponding author upon reasonable request.

## References

- [1] D. Pinto, M. Alshahrani, R. Chapurlat, T. Chevalley, E. Dennison, B.M. Camargos, A. Papaioannou, S. Silverman, J.F. Kaux, N.E. Lane, J. Morales Torres, J. Paccou, R. Rizzoli, O. Bruyere, The global approach to rehabilitation following an osteoporotic fragility fracture: A review of the rehabilitation working group of the International Osteoporosis Foundation (IOF) committee of scientific advisors, *Osteoporos Int* 33(3) (2022) 527-540.
- [2] P. García-García, R. Reyes, E. Pérez-Herrero, M.R. Arnau, C. Évora, A. Delgado, Alginate-hydrogel versus alginate-solid system. Efficacy in bone regeneration in osteoporosis, *Mater Sci Eng C Mater Biol Appl* 115 (2020) 111009.
- [3] I.R. Suhito, Y. Han, J. Min, H. Son, T.H. Kim, In situ label-free monitoring of human adipose-derived mesenchymal stem cell differentiation into multiple lineages, *Biomaterials* 154 (2018) 223-233.
- [4] Q. Huang, Y. Zou, M.C. Arno, S. Chen, T. Wang, J. Gao, A.P. Dove, J. Du, Hydrogel scaffolds for differentiation of adipose-derived stem cells, *Chem Soc Rev* 46(20) (2017) 6255-6275.
- [5] W. Yan, C. Lin, Y. Guo, Y. Chen, Y. Du, W.B. Lau, Y. Xia, F. Zhang, R. Su, E. Gao, Y. Wang, C. Li, R. Liu, X.L. Ma, L. Tao, N-Cadherin Overexpression Mobilizes the Protective Effects of Mesenchymal Stromal Cells Against Ischemic Heart Injury Through a beta-Catenin-Dependent Manner, *Circ Res* 126(7) (2020) 857-874.
- [6] J. Leong, Y.T. Hong, Y.F. Wu, E. Ko, S. Dvoretzkiy, J.Y. Teo, B.S. Kim, K. Kim, H. Jeon, M. Boppart, Y.Y. Yang, H. Kong, Surface Tethering of Inflammation-Modulatory Nanostimulators to Stem Cells for Ischemic Muscle Repair, *ACS Nano* 14(5) (2020) 5298-5313.
- [7] D. Zhang, N. Ni, Y. Wang, Z. Tang, H. Gao, Y. Ju, N. Sun, X. He, P. Gu, X. Fan, CircRNA-vgll3 promotes osteogenic differentiation of adipose-derived mesenchymal stem cells via modulating miRNA-dependent integrin  $\alpha 5$  expression, *Cell Death Differ* 28(1) (2021) 283-302.
- [8] B. Sun, R. Qu, T. Fan, Y. Yang, X. Jiang, A.U. Khan, Z. Zhou, J. Zhang, K. Wei, J. Ouyang, J. Dai, Actin polymerization state regulates osteogenic differentiation in human adipose-derived stem cells, *Cell Mol Biol Lett* 26(1) (2021) 15.
- [9] L.F.R. Gebert, I.J. MacRae, Regulation of microRNA function in animals, *Nat Rev Mol Cell Biol* 20(1) (2019) 21-37.
- [10] J. Krol, I. Loedige, W. Filipowicz, The widespread regulation of microRNA biogenesis, function and decay, *Nat Rev Genet* 11(9) (2010) 597-610.
- [11] T.X. Lu, M.E. Rothenberg, MicroRNA, *J Allergy Clin Immunol* 141(4) (2018) 1202-1207.
- [12] M.S. Vieira, A.K. Santos, R. Vasconcellos, V.A.M. Goulart, R.C. Parreira, A.H. Kihara, H. Ulrich, R.R. Resende, Neural stem cell differentiation into mature neurons: Mechanisms of regulation and biotechnological applications, *Biotechnol Adv* 36(7) (2018) 1946-1970.
- [13] R. Rupaimoole, F.J. Slack, MicroRNA therapeutics: towards a new era for the management of cancer and other diseases, *Nat Rev Drug Discov* 16(3) (2017) 203-222.
- [14] Y. Zhong, X. Li, F. Wang, S. Wang, X. Wang, X. Tian, S. Bai, D. Miao, J. Fan, Emerging Potential of Exosomes on Adipogenic Differentiation of Mesenchymal Stem Cells, *Front Cell Dev Biol* 9 (2021) 649552.

- [15] Q. Xie, Z. Wang, H. Zhou, Z. Yu, Y. Huang, H. Sun, X. Bi, Y. Wang, W. Shi, P. Gu, X. Fan, The role of miR-135-modified adipose-derived mesenchymal stem cells in bone regeneration, *Biomaterials* 75 (2016) 279-294.
- [16] C. Yang, X. Liu, K. Zhao, Y. Zhu, B. Hu, Y. Zhou, M. Wang, Y. Wu, C. Zhang, J. Xu, Y. Ning, D. Zou, miRNA-21 promotes osteogenesis via the PTEN/PI3K/Akt/HIF-1 $\alpha$  pathway and enhances bone regeneration in critical size defects, *Stem Cell Res Ther* 10(1) (2019) 65.
- [17] T. Xu, Y. Luo, J. Wang, N. Zhang, C. Gu, L. Li, D. Qian, W. Cai, J. Fan, G. Yin, Exosomal miRNA-128-3p from mesenchymal stem cells of aged rats regulates osteogenesis and bone fracture healing by targeting Smad5, *J Nanobiotechnology* 18(1) (2020) 47.
- [18] Y. Li, F. Yang, M. Gao, R. Gong, M. Jin, T. Liu, Y. Sun, Y. Fu, Q. Huang, W. Zhang, S. Liu, M. Yu, G. Yan, C. Feng, M. He, L. Zhang, F. Ding, W. Ma, Z. Bi, C. Xu, Y. Yuan, B. Cai, L. Yang, miR-149-3p Regulates the Switch between Adipogenic and Osteogenic Differentiation of BMSCs by Targeting FTO, *Mol Ther Nucleic Acids* 17 (2019) 590-600.
- [19] V. Fulci, S. Chiaretti, M. Goldoni, G. Azzalin, N. Carucci, S. Tavolaro, L. Castellano, A. Magrelli, F. Citarella, M. Messina, R. Maggio, N. Peragine, S. Santangelo, F.R. Mauro, P. Landgraf, T. Tuschl, D.B. Weir, M. Chien, J.J. Russo, J. Ju, R. Sheridan, C. Sander, M. Zavolan, A. Guarini, R. Foà, G. Macino, Quantitative technologies establish a novel microRNA profile of chronic lymphocytic leukemia, *Blood* 109(11) (2007) 4944-51.
- [20] M. Estep, D. Armistead, N. Hossain, H. Elarainy, Z. Goodman, A. Baranova, V. Chandhoke, Z.M. Younossi, Differential expression of miRNAs in the visceral adipose tissue of patients with non-alcoholic fatty liver disease, *Aliment Pharmacol Ther* 32(3) (2010) 487-97.
- [21] C.L. Dong, H.Z. Liu, Z.C. Zhang, H.L. Zhao, H. Zhao, Y. Huang, J.H. Yao, T.S. Sun, The influence of MicroRNA-150 in Osteoblast Matrix Mineralization, *J Cell Biochem* 116(12) (2015) 2970-9.
- [22] N. Wang, Z. Zhou, T. Wu, W. Liu, P. Yin, C. Pan, X. Yu, TNF- $\alpha$ -induced NF- $\kappa$ B activation upregulates microRNA-150-3p and inhibits osteogenesis of mesenchymal stem cells by targeting  $\beta$ -catenin, *Open Biol* 6(3) (2016).
- [23] X. Li, Y. Zhao, X. Li, Q. Wang, Q. Ao, X. Wang, X. Tian, H. Tong, D. Kong, S. Chang, S. Bai, J. Fan, MicroRNA-150 Modulates Adipogenic Differentiation of Adipose-Derived Stem Cells by Targeting Notch3, *Stem Cells Int* 2019 (2019) 2743047.
- [24] S. Artavanis-Tsakonas, M.D. Rand, R.J. Lake, Notch signaling: cell fate control and signal integration in development, *Science* 284(5415) (1999) 770-6.
- [25] T. Shan, J. Liu, W. Wu, Z. Xu, Y. Wang, Roles of Notch Signaling in Adipocyte Progenitor Cells and Mature Adipocytes, *J Cell Physiol* 232(6) (2017) 1258-1261.
- [26] K. Wei, I. Korsunsky, J.L. Marshall, A. Gao, G.F.M. Watts, T. Major, A.P. Croft, J. Watts, P.E. Blazar, J.K. Lange, T.S. Thornhill, A. Filer, K. Raza, L.T. Donlin, C.W. Siebel, C.D. Buckley, S. Raychaudhuri, M.B. Brenner, Notch signalling drives synovial fibroblast identity and arthritis pathology, *Nature* 582(7811) (2020) 259-264.
- [27] C. Talora, S. Cialfi, C. Oliviero, R. Palermo, M. Pascucci, L. Frati, A. Vacca, A. Gulino, I. Screpanti, Cross talk among Notch3, pre-TCR, and Tal1 in T-cell development and leukemogenesis, *Blood* 107(8) (2006) 3313-20.
- [28] C. Talora, A.F. Campese, D. Bellavia, M. Pascucci, S. Checquolo, M. Groppioni, L. Frati, H. von Boehmer, A. Gulino, I. Screpanti, Pre-TCR-triggered ERK signalling-dependent downregulation of E2A activity in Notch3-induced T-cell lymphoma, *EMBO Rep* 4(11) (2003)

1067-72.

- [29] M. Masiero, S. Minuzzo, I. Pusceddu, L. Moserle, L. Persano, V. Agnusdei, V. Tosello, G. Basso, A. Amadori, S. Indraccolo, Notch3-mediated regulation of MKP-1 levels promotes survival of T acute lymphoblastic leukemia cells, *Leukemia* 25(4) (2011) 588-98.
- [30] I. Nakamura, L. Lipfert, G.A. Rodan, T.D. Le, Convergence of alpha(v)beta(3) integrin- and macrophage colony stimulating factor-mediated signals on phospholipase Cgamma in pre-fusion osteoclasts, *J Cell Biol* 152(2) (2001) 361-73.
- [31] V.W. Wong, K.C. Rustad, S. Akaishi, M. Sorkin, J.P. Glotzbach, M. Januszyk, E.R. Nelson, K. Levi, J. Paterno, I.N. Vial, A.A. Kuang, M.T. Longaker, G.C. Gurtner, Focal adhesion kinase links mechanical force to skin fibrosis via inflammatory signaling, *Nat Med* 18(1) (2011) 148-52.
- [32] L. Liu, X. Gao, X. Li, G. Zhu, N. Li, X. Shi, Y. Wang, Calcium alendronate-coated composite scaffolds promote osteogenesis of ADSCs via integrin and FAK/ERK signalling pathways, *J Mater Chem B* 8(31) (2020) 6912-6924.
- [33] D. Ilić, Y. Furuta, S. Kanazawa, N. Takeda, K. Sobue, N. Nakatsujii, S. Nomura, J. Fujimoto, M. Okada, T. Yamamoto, Reduced cell motility and enhanced focal adhesion contact formation in cells from FAK-deficient mice, *Nature* 377(6549) (1995) 539-44.
- [34] R. McBeath, D.M. Pirone, C.M. Nelson, K. Bhadriraju, C.S. Chen, Cell shape, cytoskeletal tension, and RhoA regulate stem cell lineage commitment, *Dev Cell* 6(4) (2004) 483-95.
- [35] W.R. Thompson, C. Guilluy, Z. Xie, B. Sen, K.E. Brobst, S.S. Yen, G. Uzer, M. Styner, N. Case, K. Burrige, J. Rubin, Mechanically activated Fyn utilizes mTORC2 to regulate RhoA and adipogenesis in mesenchymal stem cells, *Stem Cells* 31(11) (2013) 2528-37.
- [36] R.W. Tilghman, J.T. Parsons, Focal adhesion kinase as a regulator of cell tension in the progression of cancer, *Semin Cancer Biol* 18(1) (2008) 45-52.
- [37] A. Woods, G. Wang, F. Beier, RhoA/ROCK signaling regulates Sox9 expression and actin organization during chondrogenesis, *J Biol Chem* 280(12) (2005) 11626-34.
- [38] V. Ambros, The functions of animal microRNAs, *Nature* 431(7006) (2004) 350-5.
- [39] Y. Tian, J. Liu, X. Bai, X. Tan, Y. Cao, K. Qin, Z. Zhao, Y. Zhang, MicroRNA expression profile of surgical removed mandibular bone tissues from patients with mandibular prognathism, *J Surg Res* 198(1) (2015) 127-34.
- [40] F.M. Moussa, B.P. Cook, G.R. Sondag, M. DeSanto, M.S. Obri, S.E. McDermott, F.F. Safadi, The role of miR-150 regulates bone cell differentiation and function, *Bone* 145 (2021) 115470.
- [41] D.M. Breitkopf, V. Jankowski, K. Ohl, J. Hermann, D. Hermert, K. Tenbrock, X. Liu, I.V. Martin, J. Wang, F. Groll, E. Gröne, J. Floege, T. Ostendorf, T. Rauen, U. Raffetseder, The YB-1:Notch-3 axis modulates immune cell responses and organ damage in systemic lupus erythematosus, *Kidney Int* 97(2) (2020) 289-303.
- [42] Y. Maekawa, S. Tsukumo, S. Chiba, H. Hirai, Y. Hayashi, H. Okada, K. Kishihara, K. Yasutomo, Delta1-Notch3 interactions bias the functional differentiation of activated CD4+ T cells, *Immunity* 19(4) (2003) 549-59.
- [43] S.W. Choi, S.U. Lee, E.H. Kim, S.J. Park, I. Choi, T.D. Kim, S.H. Kim, Osteoporotic bone of miR-150-deficient mice: Possibly due to low serum OPG-mediated osteoclast activation, *Bone reports* 3 (2015) 5-10.
- [44] M. Ebrahimi, M.G. Botelho, S.V. Dorozhkin, Biphasic calcium phosphates bioceramics

- (HA/TCP): Concept, physicochemical properties and the impact of standardization of study protocols in biomaterials research, *Mater Sci Eng C Mater Biol Appl* 71 (2017) 1293-1312.
- [45] S.E. Lobo, R. Glickman, W.N. da Silva, T.L. Arinzeh, I. Kerkis, Response of stem cells from different origins to biphasic calcium phosphate bioceramics, *Cell Tissue Res* 361(2) (2015) 477-95.
- [46] S. Miyamoto, H. Teramoto, O.A. Coso, J.S. Gutkind, P.D. Burbelo, S.K. Akiyama, K.M. Yamada, Integrin function: molecular hierarchies of cytoskeletal and signaling molecules, *J Cell Biol* 131(3) (1995) 791-805.
- [47] A.A. Saidova, I.A. Vorobjev, Lineage Commitment, Signaling Pathways, and the Cytoskeleton Systems in Mesenchymal Stem Cells, *Tissue Eng Part B Rev* 26(1) (2020) 13-25.

## Figure Captions

**Figure 1.** The expression of *miR-150-5p* in adipose-derived mesenchymal stem cells (ADSCs) during osteogenesis. Real-time PCR analysis of *miR-150* expression in ADSCs with osteogenic induction at different time points. U6 was used as the internal control.  $n = 3$ . \* $P < 0.05$ , \*\* $P < 0.01$  and \*\*\* $P < 0.001$  vs. day 0.

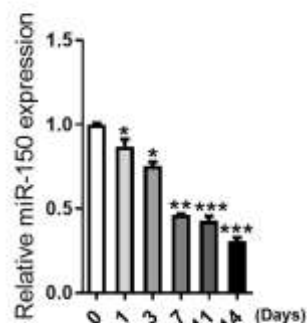


**Figure 2.** *MiR-150-5p* inhibited the osteogenic differentiation of ADSCs. **(A).** Western blot analysis of COL1A1, Runt-related transcription factor 2 (RUNX-2) and Osteocalcin in ADSCs with *miR-150-5p* overexpression after 7 days of osteogenic differentiation.  $n=3$ .  $*P < 0.05$ ,  $**P < 0.01$  and  $****P < 0.0001$  vs. Normal.  $\#P < 0.05$ ,  $\#\#P < 0.01$  and  $\#\#\#\#P < 0.0001$  vs. NC+OM. **(B).** Alkaline phosphatase (ALP) activity and ALP staining in ADSCs with *miR-150-5p* overexpression after 7 days of osteogenic differentiation.  $n=3$ .  $**P < 0.01$  vs. Normal.  $\#P < 0.05$  vs. NC+OM. Scale bar, 100 $\mu$ m. **(C).** Western blot analysis of COL1A1, RUNX-2 and Osteocalcin in ADSCs with *miR-150-5p* inhibition after 7 days of osteogenic differentiation.  $n=3$ .  $*P < 0.05$ ,  $**P < 0.01$  and  $****P < 0.0001$  vs. Normal.  $\#P < 0.05$  vs. NC+OM. **(D).** ALP activity and ALP staining in ADSCs with *miR-150-5p* inhibition after 7 days of osteogenic differentiation.  $n = 3$ .  $***P < 0.001$  vs. Normal.  $\#\#P < 0.01$  vs. NC+OM. Scale bar, 100 $\mu$ m. NC, Negative control; OM, osteogenic induced medium.

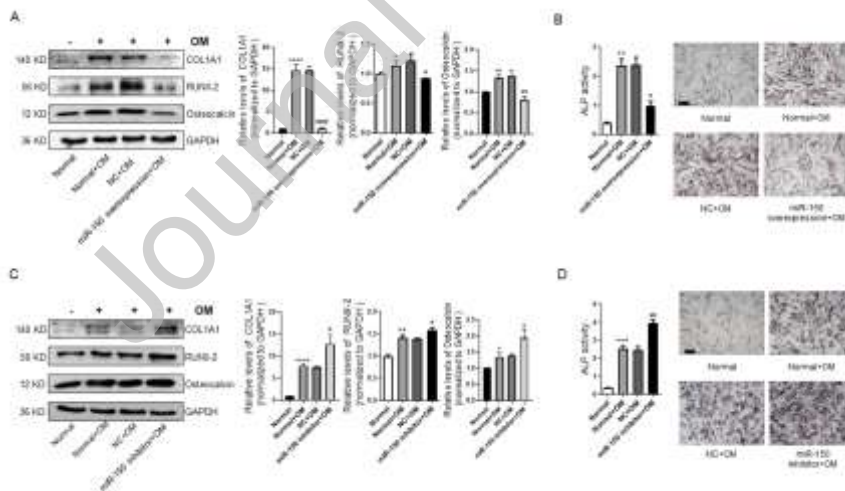


**Figure 3.** *MiR-150-5p* inhibition promoted bone formation *in vivo*. Different transfected ADSCs implanted with hydroxyapatite/tricalcium phosphate (HA/TCP) in BALB/C-nu/nu mice. **(A)**. GFP labeled ADSCs mixed with the HA/TCP powder. Scale bar, 100  $\mu$ m. **(B)**. Schematic diagram of implantation. **(C)**. Representative microcomputed tomography (micro-CT) image of the coronal section. Scale bar, 500 $\mu$ m. The red circle indicates the implant in the dorsal surface of BALB/C-nu/nu mice. **(D)**. Bone volume/tissue volume (BV/TV) analysis of implants.  $n = 3$ .  $*P < 0.05$  and  $**P < 0.01$  vs. NC.  $##P < 0.01$  vs. *shR-Notch3*. Scale bar, 500 $\mu$ m.

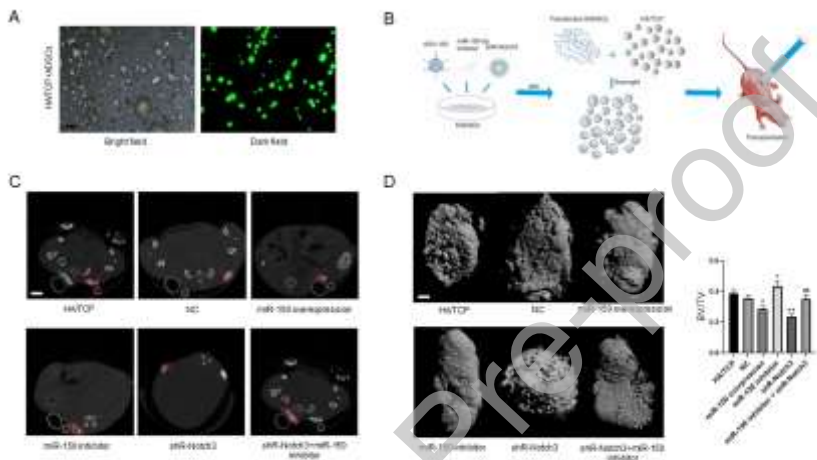


**Figure 4.** Histological staining of the implants. **(A).** Representative images of HE, Masson's trichrome, and immunostaining of COL1A1 and RUNX-2 in implants sections. Scale bar, 100  $\mu$ m. COL1A1 and RUNX-2 were stained brown. The arrow indicates the positive staining. **(B).** Collagen volume fraction (CVF) analysis of Masson's trichrome. \* $P < 0.05$ , \*\* $P < 0.01$ , \*\*\* $P < 0.001$  vs. HA/TCP. ### $P < 0.001$  vs. *miR-150* overexpression NC. \*\* $P < 0.01$  vs. *miR-150* inhibitor NC. & $P < 0.05$  vs. shR-NC. %%% $P < 0.001$  vs. shR-Notch3. **(C).** Semiquantitative analysis was used to determine COL1A1 and RUNX-2 levels of implants. \*\*\* $P < 0.001$ , \*\*\*\* $P < 0.0001$  vs. HA/TCP. ## $P < 0.01$ , ### $P < 0.001$  vs. *miR-150* overexpression NC. + $P < 0.05$ , +++ $P < 0.001$  vs. *miR-150* inhibitor NC. && $P < 0.01$  vs. shR-NC. %%% $P < 0.001$  vs. shR-Notch3.  $n=4-6$ .

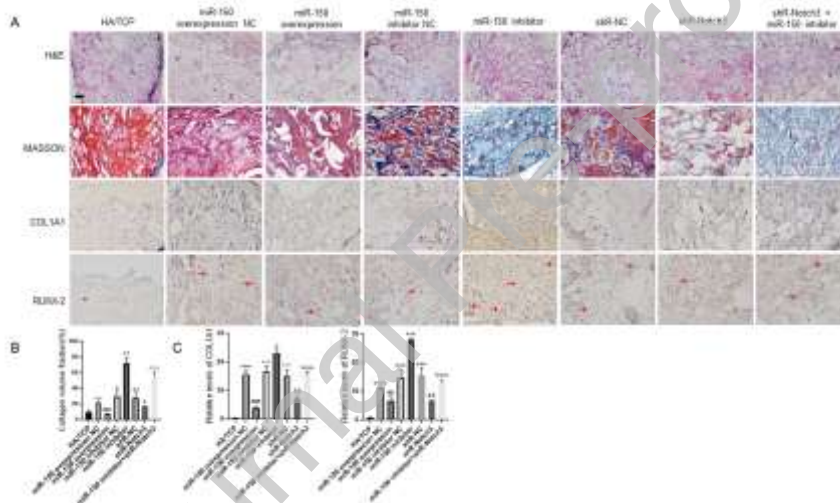


**Figure 5.** *MiR-150-5p* regulated the expression of Notch3, FAK/ERK, and RhoA in ADSCs. **(A).** Western blot analysis of Notch3, pFAK, FAK, pERK1/2, ERK1/2, and RhoA in ADSCs with *miR-150-5p* overexpression.  $n=3$ . \* $P < 0.05$  and \*\* $P < 0.01$  vs. NC. **B.** Western blot analysis of Notch3, pFAK, FAK, pERK1/2, ERK1/2, and RhoA in ADSCs with *miR-150-5p* inhibition.  $n=3$ . \* $P < 0.05$  and \*\* $P < 0.01$  vs. NC. NC, Negative control.

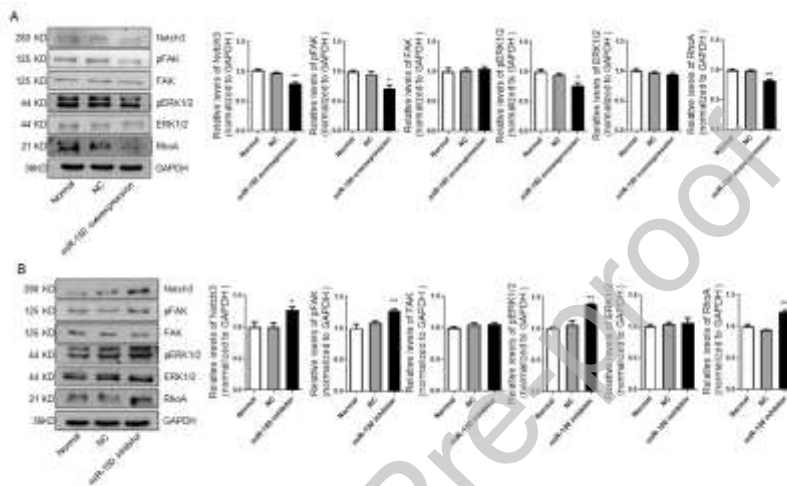


**Figure 6.** Notch3 knockdown inhibited the osteogenic differentiation of ADSCs by downregulating FAK/ERK and RhoA. **(A).** ADSCs were infected with short hairpin RNA (shRNA) lentiviruses and selected with puromycin for 1 week. Scale bar, 100  $\mu$ m. Western blot analysis of Notch3 in ADSCs with Notch3 knockdown.  $n=3$ .  $*P < 0.05$  vs. NC. **(B).** Western blot analysis of pFAK, FAK, pERK1/2, ERK1/2, and RhoA in ADSCs with Notch3 knockdown.  $n=3$ .  $*P < 0.05$ ,  $**P < 0.01$  vs. NC. **(C).** Western blot analysis of COL1A1, RUNX-2 and Osteocalcin in ADSCs with Notch3 knockdown after 7 days of osteogenic differentiation.  $n=3$ .  $*P < 0.05$ ,  $***P < 0.0001$  vs. Normal.  $\#P < 0.05$ ,  $\#\#P < 0.01$ ,  $\#\#\#\#P < 0.0001$  vs. NC+OM. **(D).** ALP activity and ALP staining in ADSCs with *miR-150-5p* overexpression after 7 days of osteogenic differentiation.  $n=3$ .  $**P < 0.01$  vs. Normal.  $\#P < 0.05$ ,  $\#\#P < 0.01$  vs. NC+OM. Scale bar, 100  $\mu$ m. NC, Negative control; OM, osteogenic induced medium.

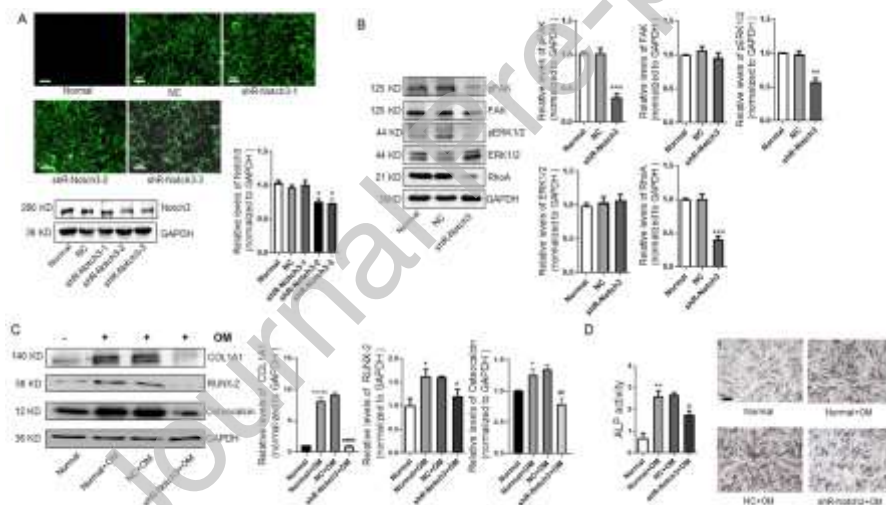


**Figure 7.** *MiR-150-5p/notch3* axis regulated osteogenesis via FAK/ERK and RhoA. **(A).** Western blot analysis of COL1A1, RUNX-2 and Osteocalcin in ADSCs after 7 days of osteogenic differentiation.  $n=3$ .  $**P < 0.01$  and  $***P < 0.001$  vs. Normal.  $\#P < 0.05$ ,  $\#\#P < 0.01$  and  $\#\#\#P < 0.001$  vs. *miR-150* inhibitor NC+shR-NC+OM.  $+P < 0.05$ ,  $++P < 0.01$  and  $+++P < 0.001$  vs. *miR-150* inhibitor NC+shR-Notch3+OM. **(B).** ALP activity and ALP staining in ADSCs after 7 days of osteogenic differentiation.  $n=3$ . Scale bar, 100  $\mu\text{m}$ .  $***P < 0.0001$  vs. Normal.  $\#\#P < 0.01$  and  $\#\#\#P < 0.001$  vs. *miR-150* inhibitor NC+shR-NC+OM.  $++P < 0.01$  vs. *miR-150* inhibitor NC+shR-Notch3+OM. **(C).** Western blot analysis of Notch3, pFAK, FAK, pERK1/2, ERK1/2 and RhoA in ADSCs.  $n=3$ .  $**P < 0.01$  and  $***P < 0.001$  vs. *miR-150* inhibitor NC+shR-NC.  $\#P < 0.05$  and  $\#\#P < 0.01$  vs. *miR-150* inhibitor NC+shR-Notch3. NC, Negative control; OM, osteogenic induced medium.

